

RESEARCH

Open Access



# Identification of three subtypes of ovarian cancer and construction of prognostic models based on immune-related genes

Wen Gao<sup>1†</sup>, Hui Yuan<sup>3†</sup>, Sheng Yin<sup>4†</sup>, Renfang Deng<sup>5\*</sup> and Zhaodong Ji<sup>2\*</sup>

## Abstract

**Background** Immunotherapy has revolutionized the treatment of ovarian cancer (OC), but different immune microenvironments often constrain the efficacy of immunotherapeutic interventions. Therefore, there is an imperative to delineate novel immune subtypes for development of efficacious immunotherapeutic strategies.

**Methods** The immune subtypes of OC were identified by consensus cluster analysis. The differences in clinical features, genetic mutations, mRNA stemness (mRNAsi) and immune microenvironments were analyzed among subtypes. Subsequently, prognostic risk models were constructed based on differentially expressed genes (DEGs) of the immune subtypes using weighted correlation network analysis.

**Results** OC patients were classified into three immune subtypes with distinct survival rates and clinical features. Different subtypes exhibited varying tumor mutation burdens, homologous recombination deficiencies, and mRNAsi levels. Significant differences were observed among immune subtypes in terms of immune checkpoint expression and immunogenic cell death. Prognostic risk models were validated as independent prognostic factors demonstrated great predictive performance for survival of OC patients.

**Conclusion** In this study, three distinct immune subtypes were identified based on gene sets related to vaccine response, with the C2 subtype exhibiting significantly worse prognosis. While no statistically significant differences in tumor mutation burden (TMB) were observed across the three subtypes, the homologous recombination deficiency (HRD) score and mRNA stemness index (mRNAsi) were notably elevated in the C2 group compared to the others. Immune infiltration analysis indicated that the C2 subtype may have an increased presence of regulatory T (Treg) cells, potentially contributing to a more favorable response to combination therapies involving PARP inhibitors and immunotherapy. These findings offer a precision medicine approach for tailoring immunotherapy in ovarian cancer patients. Moreover, the C3 subtype demonstrated significantly lower expression levels of immune checkpoint genes, a pattern validated by independent datasets, and associated with a better prognosis. Further investigation revealed

<sup>†</sup>Wen Gao, Hui Yuan and Sheng Yin contributed equally to this work.

\*Correspondence:  
Renfang Deng  
13387338586@163.com  
Zhaodong Ji  
zdji18@fudan.edu.cn

Full list of author information is available at the end of the article



© The Author(s) 2024. **Open Access** This article is licensed under a Creative Commons Attribution-NonCommercial-NoDerivatives 4.0 International License, which permits any non-commercial use, sharing, distribution and reproduction in any medium or format, as long as you give appropriate credit to the original author(s) and the source, provide a link to the Creative Commons licence, and indicate if you modified the licensed material. You do not have permission under this licence to share adapted material derived from this article or parts of it. The images or other third party material in this article are included in the article's Creative Commons licence, unless indicated otherwise in a credit line to the material. If material is not included in the article's Creative Commons licence and your intended use is not permitted by statutory regulation or exceeds the permitted use, you will need to obtain permission directly from the copyright holder. To view a copy of this licence, visit <http://creativecommons.org/licenses/by-nc-nd/4.0/>.

that the immune-related gene *FCRL5* correlates with ovarian cancer prognosis, with in vitro experiments showing that it influences the proliferation and migration of the ovarian cancer cell line SKOV3.

**Keywords** Ovarian cancer, Immunotherapy, Immune subtype, Vaccine-related genes

## Introduction

Ovarian cancer (OC) is one of the three major tumors of the gynecological reproductive system [1]. As OC lesions located deep in the female pelvic cavity are difficult to detect early, most OC patients are at a late stage at the time of first diagnosis. Cytoreductive surgery combined with platinum-based chemotherapy is an effective method for OC treatment [2]. However, the five-year survival rate of OC patients is only about 30%, and the recurrence rate is as high as 60–70% [3]. Immunotherapy has a high potential for treating advanced OC with positive effects on the prognosis [4]. Previous studies have confirmed OC as an immunogenic tumor, and tumor-infiltrating lymphocytes in the tumor tissue are positively correlated with the prognosis of OC patients [5–7]. Therefore, immunotherapy is an increasingly important option for OC treatment.

Theoretically, immunotherapy should be a viable approach for ovarian cancer, given the higher tumor mutation burden (TMB) and homologous recombination deficiency (HRD) observed in patients [8, 9]. However, clinical trial outcomes have shown that ovarian cancer patients do not respond to immunotherapy as favorably as expected. The objective response rate (ORR) to single-agent immune checkpoint blockade (ICB) such as PD-L1 or PD-1 ranges from 10–25% [10]. The relationship between PD-L1 expression and the prognosis of ovarian cancer is still controversial. Previous studies have shown that high expression of PD-L1 is common in OC patients with poor prognosis [11–13], but recent studies have shown that low expression of PD-L1 actually predicts poor prognosis of OC patients [14]. Clinically, the efficacy of immunotherapy varies significantly between individuals because of inter- and intratumoral heterogeneity of the immune microenvironment [15]. To enhance the efficacy of immunotherapy in ovarian cancer, combination therapies such as ICB with PARP inhibitors (PARPi) have been suggested [16, 17]. The proportion of immune effector cells/inhibitory cells, the location of immune cell infiltration, and the degree of immune cell activation in the tumor microenvironment are important factors affecting the prognosis and clinical immunotherapy response [18]. Therefore, the advent of CAR T-cell therapy holds promise for advancing ovarian cancer immunotherapy. Current preclinical trials are exploring the use of modified T lymphocytes targeting molecules such as NY-ESO-1, HER2, MUC16, and p53 in ovarian cancer. However, only a few researches provide comprehensive investigations about immune landscape and profiles of

OC to improve the prognosis and immune therapy of OC patients.

In this study, we identified and validated three immune subtypes of OC (C1–3) by cluster analysis based on the MSigDB database and The Cancer Genome Atlas (TCGA) database. Subsequently, we constructed risk models and screened prognostic factors based on weighted gene co-expression network analysis (WGCNA) and the differentially expressed genes (DEGs) of the immune subtypes (Fig. 1). This study not only afforded novel signatures for OC patients' prognosis, but also helped stratify and select OC patients for individual immunotherapy.

## Materials & methods

### Data acquisition

Data of The Cancer Genome Atlas ovarian cancer data collection (TCGA-OV) survival ( $n=587$ ), phenotype ( $n=758$ ), and genetic mutations were obtained from the GDC (<https://portal.gdc.cancer.gov/>). RNA-seq ( $n=379$ ) and CNV ( $n=620$ ) dataset was downloaded from UCSC Xena (<https://xenabrowser.net/>). The data set GSE26712 ( $n=195$ ) used for validation was obtained from the GEO database.

### Identification of immune subtype

A total of 347 vaccine response-related gene sets containing 13,426 genes were obtained from the C7 gene set in the MSigDB database. (<https://www.gsea-msigdb.org/gsea/MSigDB/>), of which 12,653 genes were detected to be expressed in the tumor samples of TCGA-OV dataset. Based on 12,653 genes, a Lasso-Cox regression analysis was performed on the TCGA-OV dataset using the R package glmnet (version 4.1-8). Parameters of LASSO regression (LR) are family = "cox", with random sampling and 10-fold cross-validation in the "cv.glmnet" function sets. Then 48 key survival-related genes were identified.

The R package ConsensusClusterPlus (version 1.64.0) was used for unsupervised clustering of TCGA-OV cancer samples based on these 48 key survival-related genes. The clustering algorithm was pam, and the distance was Pearson. Through comprehensive consideration of the matrix heatmap (Fig. 2A) of  $k=3$  and the consistent cumulative distribution function (CDF) map (Fig. 2B), patients of TCGA-OV were divided into three subtypes C1, C2 and C3. Ovarian cancer patients in GSE26712 data set were divided into three subtypes as well through these 48 genes. Then, the R packages survival (version 3.5-5) and survminer (version 0.4.9) were used to analyze

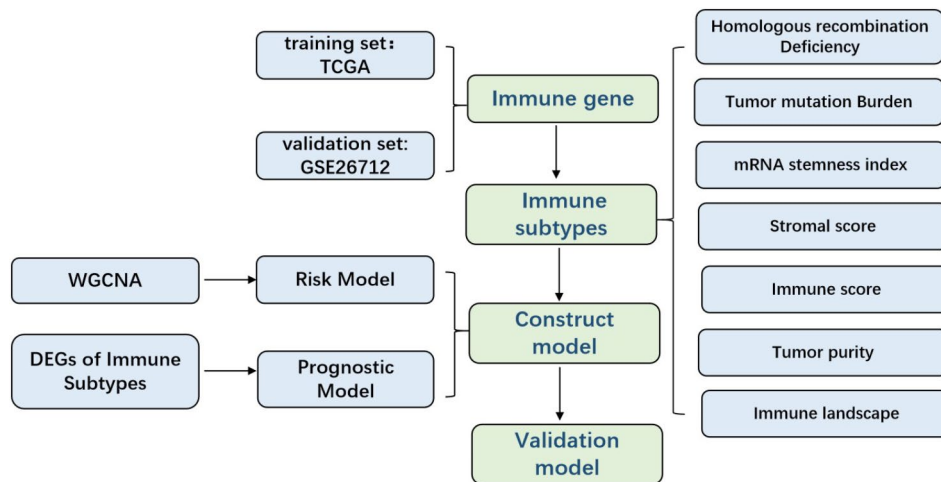


**Fig. 1** A flowchart for identifying immune subtypes and constructing prognostic risk models in ovarian cancer

the survival of the TCGA-OV subtypes and draw the Kaplan–Meier curve, respectively.

#### Analysis of genetic mutation and Copy Number Variation (CNV)

The maf file containing data on the genetic mutations of the OC cohort was downloaded from the TCGA database. Then the R package maf tools (version 2.16.0) was used to analyze and visualize the mutations. CNV frequencies and distributions were calculated manually and visualized via the R program (version 4.3.0).

#### Differential analysis of immune cells among the immune subtypes

The stromal score, immune score, and tumor purity of all TCGA-OV and GSE26712 data samples were calculated using the R package Estimate (V.1.0.13). The CYT score was defined as the geometric mean of the granzyme A (GZMA) and perforin 1 (PRF1). The CIBERSORT algorithm deduced the proportion of 22 kinds of immune cells in the sample using the expression levels of specific genes. The expression matrices of characteristic genes were first extracted from the complete expression data. Then, the R package CIBERSORT (version 1.03) was used to calculate the proportion of immune cells in all samples from TCGA-OV and GSE26712 data combined with the existing immune cell signature file. The Wilcoxon test was used to detect the difference in the proportion of immune cells in the three subtypes.

#### Immune landscape analysis

Based on the raw counts of immune-related genes in TCGA-OC, the R package monocle (version 2.28.0) analyzed the cancer samples' trajectories. The maximum group fraction was set as two and the dimension reduction algorithm was DDR Tree. The distribution of the

immune subtypes of models with different trajectories was displayed by a tree diagram. Since some immune subtypes were distributed into two different immune tracks, principal component 1 (PC1) and PC2 subdivided the immune subtype.

#### Weighted Correlation Network Analysis (WGCNA)

Weighted Gene Correlation Network Analysis (WGCNA) aims to identify co-expressed gene modules, explore the relationship between gene networks and phenotypes, and study core genes in the network. The R package WGCNA (V1.69) was used to carry out weighted co-expression network analysis of the immune-related genes to obtain different modules. The soft threshold was calculated through the pick Soft Threshold function, and the optimal soft threshold is 14. A scale-free network was constructed based on soft thresholds, and then a topological matrix was constructed, and hierarchical clustering was performed subsequently. Taking 50 as the minimum number of genes in a module, dynamically cut and identify gene modules to calculate eigengenes. The eigengenes of the modules were used for survival analysis to obtain prognostic modules. The black module was found to be associated with prognosis accompanied by a p-value of borderline significance ( $p=0.05$ ) (Fig. 7A). At the same time, the distribution differences of different module eigengenes among different subtypes were counted, and the significance of the differences was detected by the Wilcoxon test.

#### Construction of a prognostic risk model based on WGCNA

The overall survival (OS)-relevant module was selected to calculate the correlation between the gene and the module eigengenes. The genes were screened with  $R>0.9$  as the threshold, and then univariate Cox regression analysis and multivariate regression analysis were

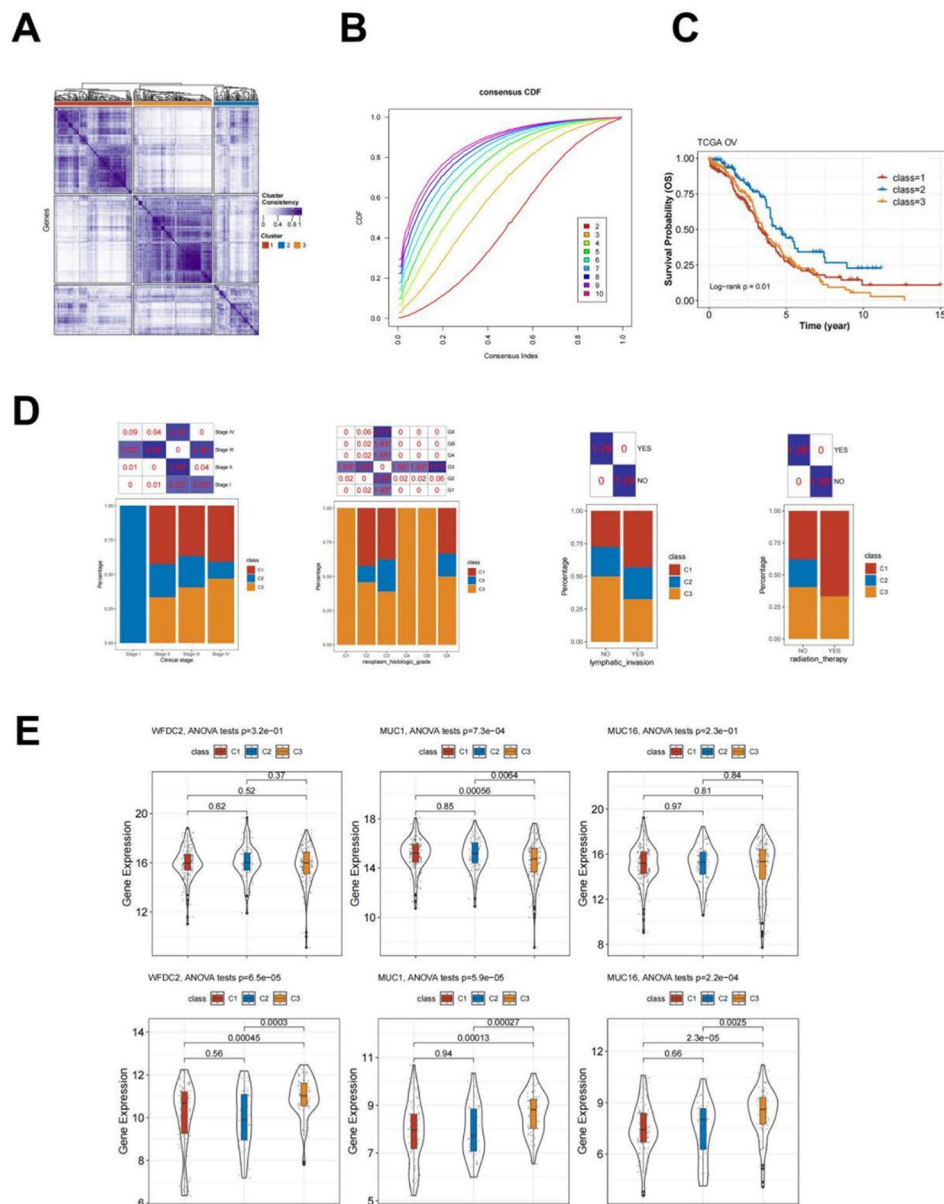


**Fig. 2** The immune subtypes and clinical signatures. **(A)** Heatmap for unsupervised consensus clustering  $k=3$  based on 48 immune-related genes of TCGA-OV dataset. **(B)** The cumulative distribution function (CDF) curve of the consensus clustering. **(C)** The overall survival curve of three subtypes according to consensus clustering in TCGA-OV cohort. **(D)** The distribution of three immune subtypes in different clinical stages and different pathological grades, as well as the distribution of these subtypes in patients with lymphoid invasion or radiotherapy. **(E)** Differential expression of WFD2, MUC1 and MUC16 in three immune phenotypes, respectively in TCGA-OV data set (top 3) and GEO26712 data set (bottom 3)

conducted for the hub genes to screen for related genes. The risk model was constructed according to the following formula:

$$\text{Risk score}_i = \sum_{(j=1)}^n \exp_{ji} * \beta_j$$

Where  $\exp$  corresponds to the gene expression,  $\beta$  represents the regression coefficient of the corresponding gene

in the multivariate regression,  $i$  represents the sample, and  $j$  represents the gene.

**Construction of a prognostic risk model based on the immune subtype DEGs**

The subtype differential genes (DEGs) in the TCGA-OV population were calculated using the R package limma (version 3.56.2). Using  $|\log FC| > 0.3$  and  $p < 0.05$  as the thresholds, a total of 163 genes were found to be differentially expressed in the three subtypes. Cox univariate

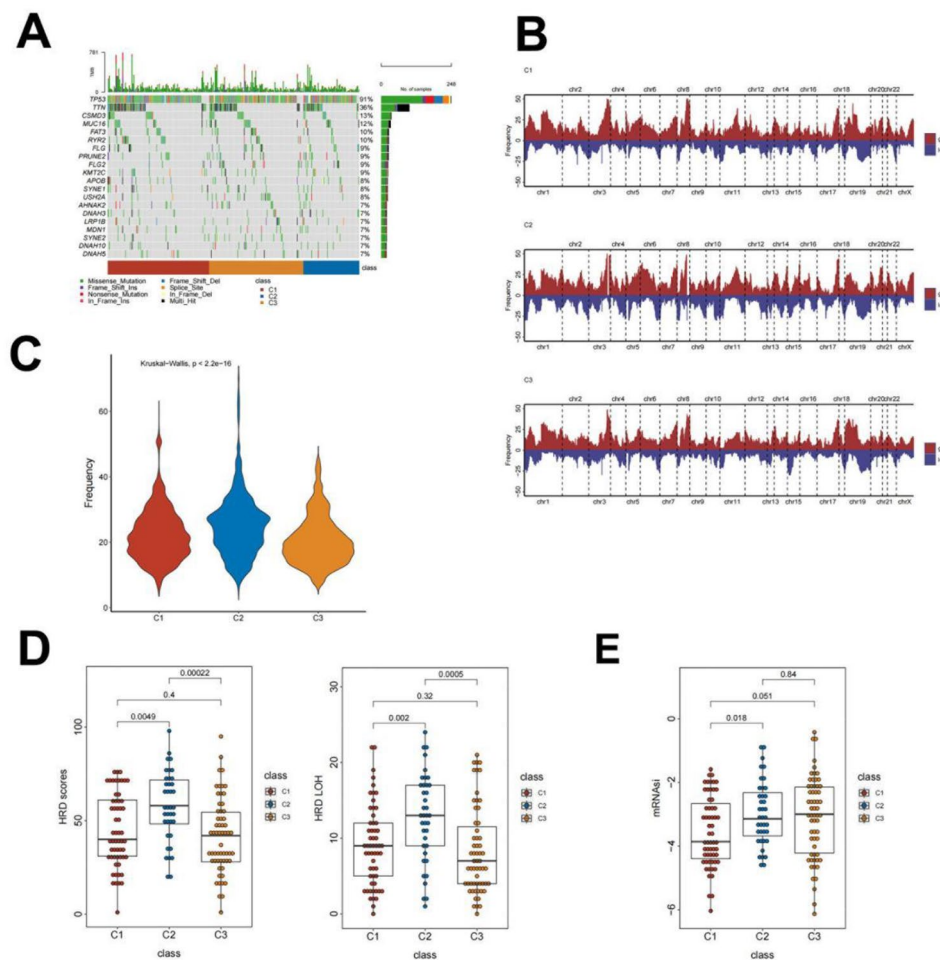


**Fig. 3** TMB, HRD, and mRNAi of the immune subtypes. **(A)** Waterfall plot depicting the top 20 mutated genes of TCGA-OV patients in three subtypes. **(B)** Copy number variation landscape across three immune subtypes, with red representing gain and blue representing loss. **(C)** Differences in total copy number variant frequencies among the three immune subtypes. **(D)** HRD scores and genomic loss of heterozygosity (LOH) scores of the three immune subtypes. **(E)** Differences in mRNAi among the three immune subtypes

regression analysis was performed on the DEGs to screen for genes with significant prognostic value. Lasso regression was performed on the results, and a risk scoring model was constructed using the R package glmnet. To build a more accurate regression model, the cross-validation method was used for lambda screening, and then the model corresponding to lambda min was selected. The expression matrix of related genes in the model was further extracted, and the risk score of each sample was calculated using the formula. The median was taken as the cutoff value, and the samples were divided into high-risk and low-risk groups.

#### Cell line and cell culture

The ovarian cancer cell lines SKOV3 was obtained from the American Type Culture Collection (ATCC) and cultured in Roswell Park Memorial Institute 1640 medium (Solarbio). All cell media were supplemented with 10%

fetal bovine serum and maintained in a humidified incubator at 37 °C with 5% CO<sub>2</sub>.

#### SiRNA transfection

The SKOV3 cells were seeded onto six-well plates at a density of  $3 \times 10^7$  cells per well and cultured until they reached a confluence of 60%. Subsequently, Lipofectamine 2000 (Invitrogen) was used for transfecting the cells with siRNAs from Sangon Biotech. After a 8 hours incubation in serum-free medium, it was replaced with medium containing 10% fetal bovine serum (FBS). Following an additional twenty-four hour incubation period, qRT-PCR analysis was carried out to assess the effectiveness of knockdown. FCRL5: siRNA-1 sense: 5'-CGGAA GUAACACUGAAUAA-3', antisense: 5'-UUAUUCAGU GUUACUCCG-3'; siRNA-2 sense: 5'-AAGAUUCUC UGCGCACUUU-3', antisense: 5'-AAAGUGCGCAGAG AAUCUU-3'; The transfected cells will be prepared for CCK-8 and transwell assays.



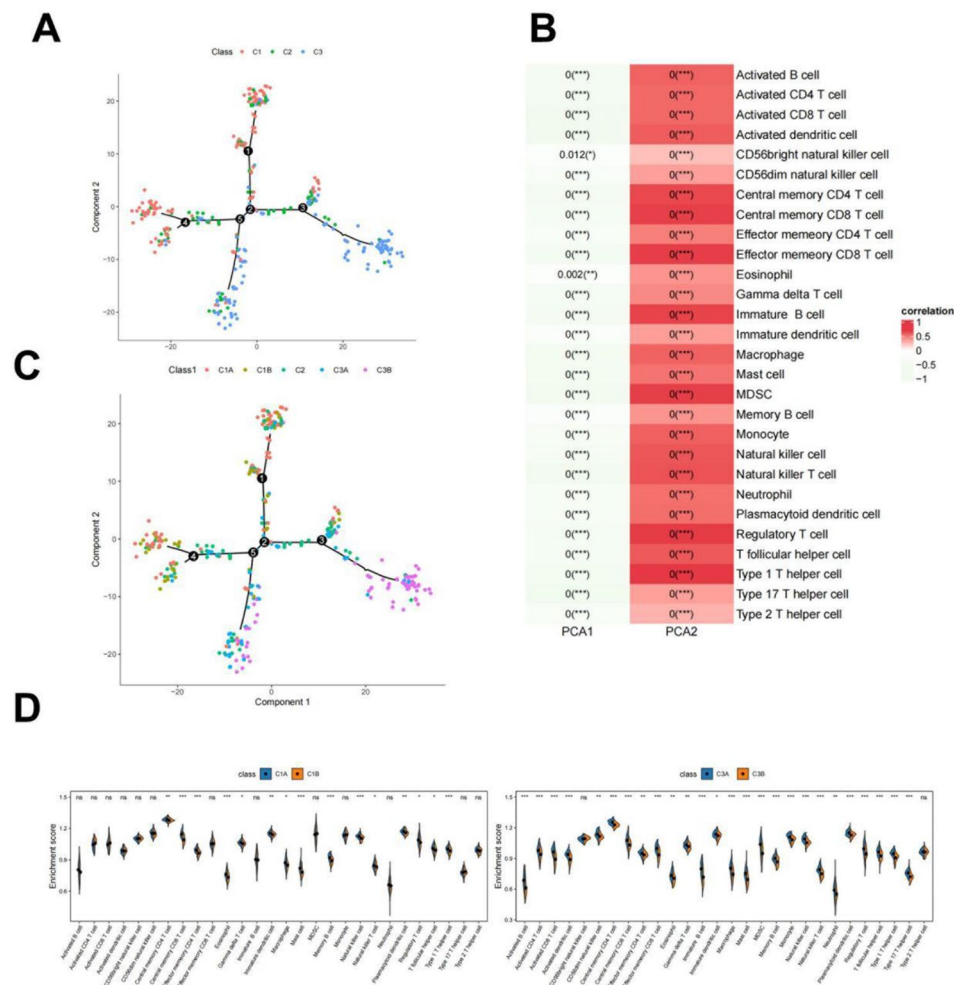


**Fig. 5** Immune cell infiltration of subtypes in ovarian cancer. **(A)** Trajectory of the TCGA-OV samples based on immune cell infiltration and distribution of the immune subtypes in the tree diagram by monocle. **(B)** Correlations between PC1/PC2 obtained by principal component analysis and 22 immune cells. **(C)** Distribution of subgroups of the immune subtypes C1 (left) and C3 (right) in the tree diagram. **(D)** Proportion of immune cells in the subgroups C1A/C1B (left) and C3A/C3B (right)

immune subtypes, demonstrating that different immune subtypes had different HRD scores (Fig. 3D). The C2 subtype showed the highest tumor mutation burden, the highest frequency of copy number variations, and the highest homologous recombination deficiency score (Fig. 3), compared to the other two subtypes. Moreover, although the TMB, types of BRCA1 and BRCA2 mutations in C2 were not significantly different from those observed in the other two groups, the specific mutation sites varied significantly (Figure S2). Additionally, the frequency of BRCA1 mutations was notably higher in the C2 compared to the other two clusters. The gene stemness features were obtained from the published literature [23], and the mRNasi was calculated based on the mRNA data of the TCGA-OV cohort. The mRNasi of C2 was significantly higher than that of C1 or C3, and there was no significant difference in other subtypes (Fig. 3E).

### Immune-related factors in immune subtypes

The immunocompetences of the immune subtypes were compared via TIP web (<http://biocc.hrbmu.edu.cn/TIP/>), and C1, C2, and C3 were significantly different in most of the immunocompetence indexes (Figure S3A). Next, we found the differential expressions of immune checkpoints (ICPs) in the three subtypes (Fig. 4A, Figure S3B), as well as immunogenic cell death (ICD)-related molecules (Fig. 4B, Figure S3C). To explore the differences in the immune cells among the immune subtypes, the stromal score, immune score, and tumor purity were calculated based on the data from TCGA-OV and GSE26172. The results showed differences between the three subtypes in immune score and tumor purity (Fig. 4C, Figure S3D). Furthermore, the three subtypes showed different percentages of infiltrating immune cells, such as T cells CD8, NK cells activated, macrophages M1, macrophages M2, and dendritic cells activated (Fig. 4D, E, Figure S3E, F).

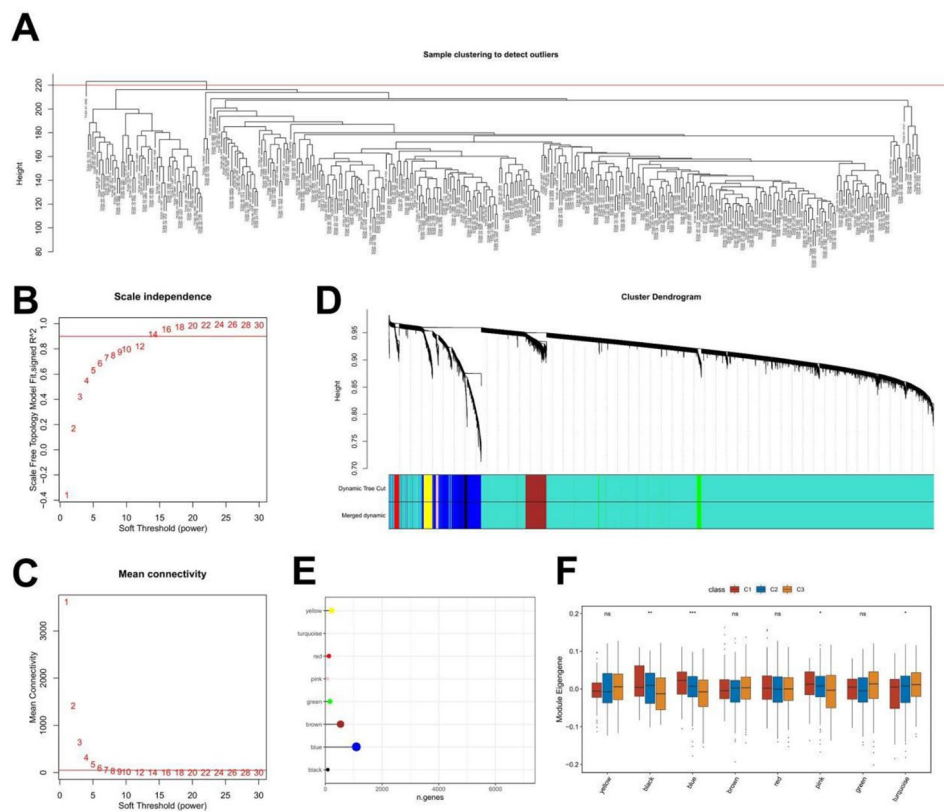


**Fig. 6** Construction of WGCNA co-expression network. **A.** Tree diagram of samples in TCGA-OV cohort. **B.** Scale-free fit index analysis of soft thresholds. **C.** The average connectivity analysis of soft thresholds. **D.** Clustering dendrogram of co-expression network analysis based on the gene hierarchical, modules were constructed and displayed in different colors. **E.** Number of genes in the module. **F.** Differences in the distribution of module eigengenes among subgroups

### Immune landscape of OC

Based on the immune-related gene matrix of TCGA-OV, Monocle software was used to analyze the trajectory of the cancer samples, and then the distribution of the immune subtypes of samples with different trajectories was displayed by a tree diagram. The tree diagram shows that each subtype was mostly in different branches (Fig. 5A). The correlation between PC1/PC2 and 22 kinds of immune cells such as different subtypes of B cells and T cells was calculated (Fig. 5B). PC1 and PC2 were used to subdivide C1, C2, and C3 because of the distribution of one immune subtype into two different branches (Fig. 5C). The results showed that C1 had a separate branch, while C1A and C1B were in the same branch, and C3A and C3B were in the same branch. The distribution of the C1A and C1B immune cells and C3A and C3B (Fig. 5D) showed differences. The enrichment score of T cell was higher in C1A compared with C1B ( $p < 0.05$ ), such as central memory CD4 T cell, central memory CD8 T cell, effector memory CD4 T cell. The enrichment score of T cells was also higher in C3A, in addition to the enrichment fraction of B cells, when compared to C3B.

### Construction of WGCNA network and risk model

WGCNA was performed based on expression of immune-related genes in TCGA-OV cohort. After soft threshold screening, a network was constructed with power 14 (Fig. 6A–E). Then, eigengenes corresponding to each sample of each module were calculated. The results showed that there were significant differences in the distribution of the module eigengenes in the immune subtypes (Fig. 6F).

Survival analysis was performed on the module using eigengenes, and the results showed that the black module was significantly correlated with prognosis (Fig. 7A). GO analysis was then performed on the black module genes (Fig. 7B).

The black module contained 71 genes, and 13 genes ( $R > 0.9$ ) were selected as hub genes. Five prognostic-related genes were obtained by univariate Cox regression analysis (Table S2), and an independent prognosis-related gene (Fc receptor-like 5, *FCRL5*) was finally accepted by stepwise regression method. The risk score of samples was calculated by a formula: risk score =  $(-0.17 * FCRL5)$ , and the median 0.0083 was used as the cutoff value to divide sample into the high/low-risk groups (Fig. 7C, D). There was a significant difference in survival rate

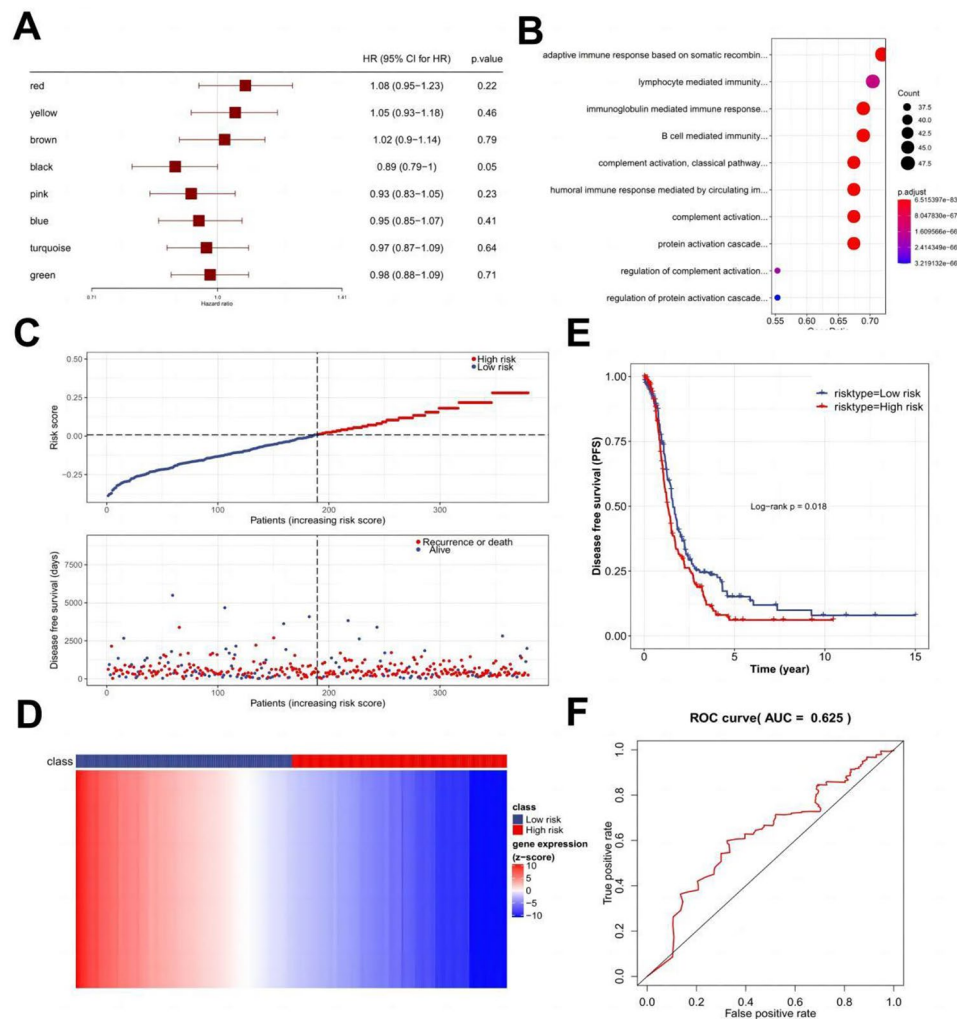


**Fig. 7** Construction of the prognostic model of ovarian cancer based on the results of WGCNA. **(A)** Univariate cox analysis with WGCNA module. **(B)** GO analysis of genes in the black module. **(C)** Distribution of risk scores (top, red represents high-risk group, blue represents low-risk group) and survival status (bottom, red represents patient death, blue represents alive) of TCGA-OV patients. **(D)** Heat map of risk score of TCGA-OV patients. **(E)** Kaplan–Meier curve of different risk groups. **(F)** ROC curve of the single gene risk model

between the high-risk and low-risk groups ( $p=0.018$ ) (Fig. 7E). The area under the receiver operating characteristic (ROC) curve (AUC) is 0.625, indicating that the model has a certain prediction efficiency (Fig. 7F). We investigated whether clinical characteristics and risk scores were associated with prognosis. First, a single-factor Cox regression analysis was performed, and the results showed that only the p-value of the risk score was less than 0.05 (Figure S5A). Multivariable cox regression analysis using these factors as covariates showed that risk score remained an independent prognostic factor for overall survival ( $p=0.008$ ) (Figure S5B).

#### Construction of the prognostic model by the immune subtype DEGs

The DEGs of the three subtypes were obtained using the R package limma, and 163 DEGs were shared by these

subtypes (Figure S4). A total of six DEGs (*RP1-67A8.3*, *IGLV3-25*, *IGHV3-13*, *IGKV3OR2-268*, *WFDC12*, and *LINC00454*) were found with significant prognostic values (Fig. 8A–B, Figure S6A–B), and we constructed a risk model based on these six genes using lasso regression (Fig. 8C–E). The risk score of TCGA-OV samples was calculated by a formula: risk score =  $(-0.11 * RP1-67A8.3) + (-0.04 * IGLV3-25) + (-0.05 * IGHV3-13) + (-0.09 * IGKV3OR2-268) + (-0.099 * WFDC12) + (0.09 * LINC00454)$ . The high- and low-risk groups were divided based on the median of calculated risk score. The Kaplan–Meier curve showed that the high-risk group had a poorer prognosis than the low-risk group (Fig. 8F). The AUC of six DEGs model was 0.734 and it was increased with the time when 1, 2, and 3 year by ROC were analyzed (Fig. 8G, Figure S6C), suggesting an excellent diagnostic value of the model. We also evaluated the risk score of

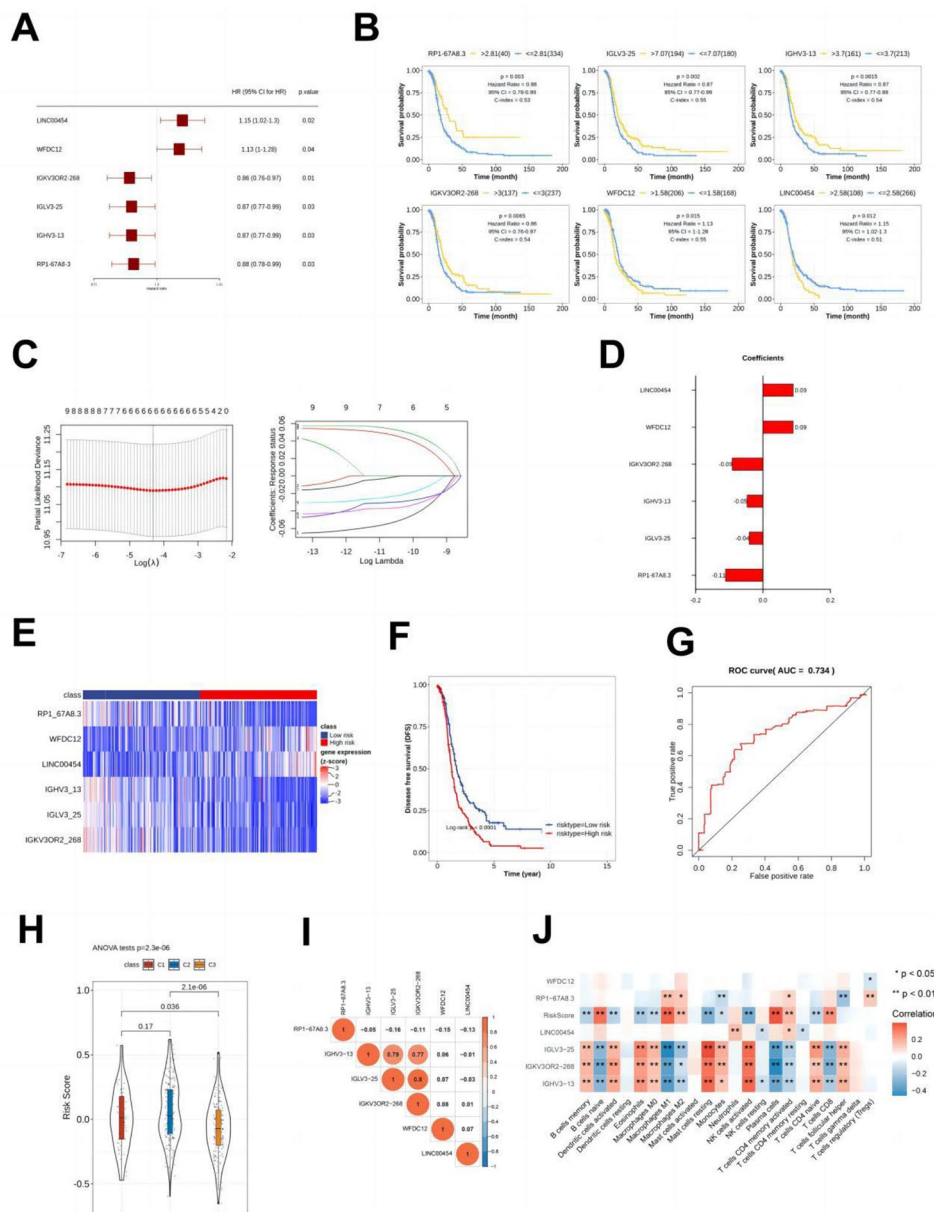


**Fig. 8** Construction of the prognostic model based on the immune subtypes. **(A)** Prognostic vaccine response related genes screened by univariate Cox regression. **(B)** Kaplan–Meier curve of six prognostic genes. **(C)** Ten-fold cross-validation error rate plot (left) and lasso regression coefficient profile (right). **(D)** Regression coefficient corresponding to the screened variables. **(E)** Heat map of genes in the lasso regression model. **(F)** Kaplan–Meier curve of high-risk and low-risk groups divided by risk score. **(G)** ROC curve of the risk model. **(H)** Differences in risk scores among three immune subtypes,  $p < 0.05$  was considered statistically significant. **(I)** Correlation between six factors of the risk model. **(J)** Association between factors of the risk model and immune infiltrating cells

the three immune subtypes and demonstrated that the C2 subtype had an overall higher risk score, while the C3 subtype had the opposite (Fig. 8H). We also used Pearson correlation analysis to examine the correlation between the six DEG members. As shown in Fig. 8I, significant positive correlations were observed between *IGHV3-13* and both *IGLV3-25* and *IGKV3OR2-268*. Finally, we confirmed the association between the expression of the six DEGs with the main infiltrating immune cells. These data

indicated that *IGHV3-13*, *IGLV3-25*, and *IGKV3OR2-268* were significantly correlated with the most significant numbers of immune cells, such as B cells, eosinophils, and T cells (Fig. 8J).

**Discussion**

In this study, we screened 48 genes significantly associated with OC prognosis from 13,426 vaccine response genes, and then identified three subtypes of OC (C1, C2,

and C3) based on these 48 prognostic signatures. Subsequently, the relationships between the subtypes and the clinical characteristics were assessed. The results demonstrated that OC patients in the C2 subtype had better survival than the two other subtypes, and the immune subtypes were connected to the clinical stage, neoplasm histological grade, and radiation therapy. This indicates that immune subtypes might affect tumorigenesis and progression of OC. WFDC2 is a novel effective biomarker for OC recurrence, and MUC1 is an ideal target for targeted therapy to control metastasis and recurrence of OC [24, 25]. The C3 subtype showed the lowest expression levels of WFDC2 and MUC1 of the three subtypes. The above results suggest that the three subtypes have different clinical features.

TMB, or the number of somatic mutations, has been widely studied as a biomarker of immunotherapy response [26]. A higher TMB increases the likelihood of tumor neoantigen production, which in turn improves immune recognition and the antitumor effects of immunotherapy [27, 28]. The C2 subtype was confirmed to have a higher CNV frequency than C1 and C3. Subsequently, we analyzed the HRD of the three subtypes, which causes the genetic mutations and TMB [29, 30]. The results suggested that the C2 subtype had a higher HRD score, indicating that C2 may respond better to combination therapies involving PARP inhibitors and immunotherapy. And the latest study utilizing single-cell gene expression profiling and T cell receptor analysis identified effector regulatory T cells (eTregs) as critical responders to homologous recombination deficiency (HRD) and neoadjuvant therapy in high-grade serous ovarian cancer (HGSOC), offering novel insights into the immunotherapeutic potential for HRD-associated tumors. Consistent with these findings, our analysis demonstrated that the C2 subtype is characterized by both elevated HRD scores and an increased fraction of Treg cells (Figure S2F), suggesting heightened sensitivity to these treatments [31].

Many inhibitory immune checkpoint proteins exist in the immune system, such as PD-1 and CTLA4. These proteins are usually derived from activated lymphocytes and tumor cell surfaces, with functions to adjust self-tolerance, prevent autoimmune reactions, and protect tissues from immune attack [32]. They can also inhibit the proliferation and activation of T cells so that cancer cells evade immune surveillance [33]. ICD is a unique cell death mode that can induce specific immunity against tumor cell antigens. This immune response can cause an increase in the number of T lymphocytes, which is strongly correlated with the prognosis after chemotherapy [34]. In this study, the C3 subtype showed the lowest gene expression of most of the ICPs, and the highest gene levels in some ICD-related molecules. Therefore, the C3

subtype has more potential to show satisfactory results after chemotherapy and immunotherapy. The survival analysis agreed with this hypothesis, confirming a better prognosis for C3 than for C1 or C2.

As an important part of the tumor microenvironment, immune cells have dual functions of immune stimulation and immunosuppression, which can promote or inhibit tumor progression [35, 36]. We found that the C3 subtype contained fewer immune cells, such as neutrophils. Tumor-infiltrating Tregs are associated with poor prognosis of OC patients [37, 38]. OC patients with a decreased ratio of neutrophils to lymphocytes have a better prognosis, probably because neutrophils in the microenvironment can promote the progression and metastasis of OC by the formation of neutrophil extracellular traps and release of cytokines and chemokines [39–41]. These results partly explain why OC patients in the C3 subtype had a better prognosis than patients in subtypes C1 and C2. The C2 subtype could be further subdivided into C2A and C2B, and there were significant differences between C2A and C2B in 21 tumor-infiltrating immune cells. This finding might account for the interesting phenomenon that C2 did not have the highest immune score but showed the worst survival.

WGCNA aims to find co-expressed gene modules, explore the correlation between gene networks and phenotypes, and dig out the core genes in the network [42]. We performed WGCNA on the immune-related genes and found that the eigengenes of the three immune subtypes differed in the black, blue, pink, and turquoise modules. Of these, the black module was significantly associated with the prognosis of OC patients. The genes in the black module were screened, and *FCRL5* was selected as an independent prognostic factor to construct the risk model. *FCRL5* is a surface protein expressed selectively on B cells and plasma cells [43]. Overexpression of *FCRL5* has been detected in skin cutaneous melanoma and multiple myeloma, but the role of *FCRL5* in OC remains unknown [43, 44]. In our study, the function of *FCRL5* in ovarian cancer cells was assessed in vitro. The results from CCK-8 and cell migration assays showed that knockdown of *FCRL5* significantly suppressed the proliferation and migration of ovarian cancer cells (Figure S7). In addition to this, the risk model based on *FCRL5* also demonstrated that the survival of patients in the high-risk group was shorter than that in the low-risk group, and showed a favorable forecast performance.

Subsequently, we screened the shared DEGs of the three immune subtypes, and six genes (*RP1\_67A8.3*, *IGLV3\_25*, *IGHV3\_13*, *IGKV3OR2\_268*, *WFDC12*, and *LINC00454*) were selected to construct a new prognostic risk model. The Kaplan–Meier curve confirmed that the patients in the high-risk group had a poorer prognosis than those in the low-risk group. The ROC curve showed

an excellent forecast performance of this risk model, with AUC of 0.734. The risk model was performed to predict the prognosis of the immune subtype. The C3 subtype had the lowest risk score, while the C2 subtype had a relatively higher risk score. The results were in accord with the survival analysis of the three subtypes and reflected the model's accuracy.

In recent years, there has been a growing interest in classifying ovarian cancer (OC) based on immune-related genes to predict patient prognosis. For instance, Ye et al. identified two immune subtypes of OC patients through hierarchical clustering using immune pathway-based analysis [43]. Lu et al. identified two immune subtypes based on 26 prognostic immunologically relevant genes [44]. However, despite these studies, there is currently no standardized classification method and discrepancies still exist regarding the biological significance and prognostic value of these immune subtypes. In contrast to previous research, our study incorporates vaccine-related genes along with immune gene expression to classify OC patients into more refined immune subtypes. This approach not only provides novel theoretical insights for future immunotherapy but also serves as a crucial reference for vaccine development and patient stratification in clinical practice. Through this study, we aim to gain a better understanding of the heterogeneity within the OC immune microenvironment and its impact on patient prognosis, ultimately facilitating the development of more precise and personalized immunotherapy strategies in future clinical practice.

Although we performed a systematic analysis on the role of the immune subtype, and cross-certified the result through different methods, the study has some limitations. Firstly, there is no information about immunotherapy in TCGA-OV, which made the study lack the confirmation of association between immune subtypes and immunotherapy. Secondly, we couldn't identify whether the immune subtype was an independent prognostic factor after the thorough adjustment of clinicopathological information. More investigations are needed to certify the prognostic and immunological value of immune subtypes and prognostic risk models.

## Conclusion

Through this study, we identified significant differences in tumor mutation burden (TMB), homologous recombination deficiency (HRD), and immune cell infiltration across different immune subtypes. This offers new perspectives for predicting patient prognosis and therapeutic response. The classification of immune subtypes in this study will help to identify OC patients suitable more precisely for immunotherapy, and in the context of vaccine development, this stratification method holds broad future potential.

## Supplementary Information

The online version contains supplementary material available at <https://doi.org/10.1186/s13048-024-01526-w>.

Supplementary Table 1: Clinicopathological associations of C1–3 in OC based on TCGA.

Supplementary Table 2: Univariate Cox regression analysis of five immune-related prognostic factors identified by WGCNA.

Supplementary Figure 1: The expression of ovarian cancer (OC) biomarkers (WFDC2, MUC1, and MUC16) by IHC (HPA) in ovarian normal tissue and ovarian cancer tissue.

Supplementary Figure 2: Tumor mutation burden (TMB), BRCA1 and BRCA2 mutations in immune subtypes. (A) Comparison of TMB among three immune subtypes (B) Comparison of the number of mutated genes among three immune subtypes. (C) Oncoplot of BRCA1 and BRCA2 mutations in samples of three immune subtypes in TCGA-OV dataset. (D) Lollipop plot of BRCA1 and BRCA2 mutation sites and types in samples of three immune subtypes.

Supplementary Figure 3: Immune-related factors in the immune subtypes. (A) Analysis of immune activity among the immune subtypes. (B) Immune checkpoints (ICPs) of the three immune subtypes in GSE26712. (C) Immunogenic cell death (ICD)-related molecules of the three immune subtypes in GSE26712. (D) Stromal score, immune score, and tumor purity of the different subtypes in GSE26712. (E) Heatmap of significantly different immune cells fractions of three subtypes in GSE26712. (F) Box plot showing differences in immune cell abundance of three subtypes in GSE26712.

Supplementary Figure 4: Differentially expressed genes in the three immune subtypes. (A) Venn diagram of differentially expressed genes among subtypes. (B) Heatmap of differential expressed genes among subtypes.

Supplementary Figure 5: Evaluation of FCRL5 single-gene model. (A) 1-, 2-, and 3-year ROC curves calculated from risk scores in the TCGA-OV dataset. (B) Forrest plots of univariate Cox regression analyses of each clinical index and risk score versus survival. (C) Forrest plots of multivariate Cox regression analyses of each clinical index and risk score versus survival.

Supplementary Figure 6: The construction of six differentially expressed genes model related to Figure 8. (A) Correlation analysis of the six DEGs in the model with immune subtypes C1–3. (B) Multivariate Cox regression analyses for the six DEGs. (C) 1-, 2-, and 3-year ROC calculated from risk scores of six DEG model in the TCGA-OV dataset.

Supplementary Figure 7: The effect of knockdown of FCRL5 on OC cell proliferation. (A) Examination of FCRL5 expression in FCRL5-knockdown cells by qRT-PCR. (B) CCK-8 assay and (C) Transwell assay of FCRL5-knockdown cells. Bars represent SD from three independent experiments. All error bars = 95 % CIs. \*P < 0.05, \*\*P < 0.01, \*\*\*P < 0.001.

## Author contributions

Wen Gao and Sheng Yin collected all data and drafted the manuscript. Zhaodong Ji and Renfang Deng participated in the project design and manuscript discussion. Hui Yuan performed the data visualization. Zhaodong Ji designed the project and edited the manuscript. Wen Gao and Zhaodong Ji helped in funding acquisition. All authors contributed to the article and approved the submitted version.

## Funding

This study was supported by grants from the Medical Health Science and Technology Project of Zhejiang Province (No.2022KY627 and 2024KY793 for Gao), the Yangfan Plan of Shanghai Science and Technology Commission (No. 22YF1404700 for Ji) and the Research Start up Fund of Huashan Hospital (No. 2021QD043 for Ji).

## Data availability

No datasets were generated or analysed during the current study.

## Declarations

### Competing interests

The authors declare no competing interests.

### Author details

<sup>1</sup>Department of Gynecologic Oncology, Zhejiang Cancer Hospital, Hangzhou Institute of Medicine (HIM), Chinese Academy of Sciences, Hangzhou, Zhejiang 310022, China

<sup>2</sup>Department of Laboratory Medicine, Huashan Hospital, Fudan University, Shanghai 200040, China

<sup>3</sup>Key Laboratory of Digital Technology in Medical Diagnostics of Zhejiang Province, Dian Diagnostics Group Co., Ltd, Hangzhou City, Zhejiang 310022, China

<sup>4</sup>Department of Obstetrics and Gynecology, Zhongshan Hospital, Fudan University, Shanghai 200032, China

<sup>5</sup>Department of Oncology, The Second Hospital of Zhuzhou City, Zhuzhou 412000, China

Received: 27 May 2024 / Accepted: 1 October 2024

Published online: 21 October 2024

## References

- Zheng MJ, Li X, Hu YX, Dong H, Gou R, Nie X, Liu Q, Ying-Ying H, Liu JJ, Lin B. Identification of molecular marker associated with ovarian cancer prognosis using bioinformatics analysis and experiments. *J Cell Physiol.* 2019;234(7):11023–36.
- Matulonis UA, Sood AK, Fallowfield L, Howitt BE, Sehouli J, Karlan B Y. ovarian cancer. *Nat Reviews Disease Primers.* 2016;2:16062.
- Ghisoni E, Imbimbo M, Zimmermann S, Valabrega G. Ovarian Cancer immunotherapy: turning up the heat. *Int J Mol Sci.* 2019;20(12):2927.
- Ventriglia J, Paciolla I, Pisano C, Cecere SC, Napoli M, Tambaro R, Califano D, Losito S, Scognamiglio G, Setola SV. Immunotherapy in ovarian, endometrial and cervical cancer: state of the art and future perspectives. *Cancer Treat Rev.* 2017;59:109–16.
- Drakes ML, Stiff PJ. Regulation of Ovarian Cancer Prognosis by Immune cells in the Tumor Microenvironment. *Cancers.* 2018;10(9):302.
- Tu L, Guan R, Yang H, Zhou Y, Hong W, Ma L, Zhao G, Yu M. Assessment of the expression of the immune checkpoint molecules PD-1, CTLA4, TIM-3 and LAG-3 across different cancers in relation to treatment response, tumor-infiltrating immune cells and survival. *Int J Cancer.* 2020;147(2):423–439.
- Zeng Y, Li B, Liang Y, Reeves PM, Qu X, Ran C, Liu Q, Callahan MV, Sluder AE, Gelfand JA, Chen H, Poznansky MC. Dual blockade of CXCL12-CXCR4 and PD-1-PD-L1 pathways prolongs survival of ovarian tumor-bearing mice by prevention of immunosuppression in the tumor microenvironment. *FASEB J.* 2019;33(5):6596–608.
- Wall JA, Meza-Perez S, Scalise CB, Katre A, Londono AI, Turbitt WJ, Randall T, Norian LA, Arend RC. Manipulating the Wnt/beta-catenin signaling pathway to promote anti-tumor immune infiltration into the TME to sensitize ovarian cancer to ICB therapy. *Gynecol Oncol.* 2021;160(1):285–94.
- Cancer Genome Atlas Research N. Integrated genomic analyses of ovarian carcinoma. *Nature.* 2011;474(7353):609–15.
- Varga A, Piha-Paul S, Ott PA, Mehnert JM, Berton-Rigaud D, Morosky A, Yang P, Ruman J, Matei D. Pembrolizumab in patients with programmed death ligand 1-positive advanced ovarian cancer: analysis of KEYNOTE-028. *Gynecol Oncol.* 2019;152(2):243–50.
- Ledermann JA, Embleton AC, Raja F, Perren TJ, Jayson GC, Rustin G, Kaye SB, Hirte H, Eisenhauer E, Vaughan M. Cediranib in patients with relapsed platinum-sensitive ovarian cancer (ICON6): a randomised, double-blind, placebo-controlled phase 3 trial. *Lancet.* 2016;387(10023):1066–74.
- Wan C, Keany MP, Dong H, Al-Alem LF, Hill SJ. Enhanced efficacy of simultaneous PD-1 and PD-L1 immune checkpoint blockade in high grade serous ovarian cancer. *Cancer Res.* 2020;81(1):158–73.
- Xue C, Xu Y, Ye W, Xie Q, Gao H, A B X, Zhang D, Jiang J. Expression of PD-L1 in ovarian cancer and its synergistic antitumor effect with PARP inhibitor. *Gynecol Oncol.* 2020;157(1):222–33.
- Tan D, Sheng L, Yi QH. Correlation of PD-1/PD-L1 polymorphisms and expressions with clinicopathologic features and prognosis of ovarian cancer. *Cancer Biomark.* 2018;21(2):287–97.
- Zhou Q, Yan X, Liu W, Yin W, Ren C. Three Immune-Associated subtypes of diffuse glioma Differ in Immune Infiltration, Immune Checkpoint molecules, and prognosis. *Front Oncol.* 2020;10:586019.
- Musacchio L, Cicala CM, Camarda F, Ghizzoni V, Giudice E, Carbone MV, Ricci C, Perri MT, Tronconi F, Gentile M, Salutati V, Scambia G, Lorusso D. combining PARP inhibition and immune checkpoint blockade in ovarian cancer patients: a new perspective on the horizon? *ESMO Open.* 2022;7(4):100536.
- Maiorano BA, Lorusso D, Maiorano MFP, Ciardiello D, Parrella P, Petracca A, Cormio G, Maiello E. The interplay between PARP inhibitors and Immunotherapy in Ovarian Cancer: the Rationale behind a New Combination Therapy. *Int J Mol Sci.* 2022;23(7).
- Petitprez F, Meylan M, Reyniès A, d, Sautès-Fridman C, Fridman W H. The Tumor Microenvironment in the response to Immune Checkpoint Blockade therapies. *Front Immunol.* 2020;11:784.
- Scaletta G, Plotti F, Luvero D, Capriglione S, Montera R, Miranda A, Lopez S, Terranova C, Carlo DCN, Angioli R. The role of novel biomarker HE4 in the diagnosis, prognosis and follow-up of ovarian cancer: a systematic review. *Expert Rev Anticancer Ther.* 2017;17(9):827–39.
- Abkevich V, Timms KM, Hennessy BT, Potter J, Carey MS, Meyer LA, Smith-McCune K, Broaddus R, Lu KH, Chen J. Patterns of genomic loss of heterozygosity predict homologous recombination repair defects in epithelial ovarian cancer. *Br J Cancer.* 2012;107(10):1776–82.
- Birkbak NJ, Wang ZC, Kim J-Y, Eklund AC, Li Q, Tian R, Bowman-Colin C, Li Y, Greene-Colozz A. Telomeric allelic imbalance indicates defective DNA repair and sensitivity to DNA-damaging agents. *Cancer Discov.* 2012;2(4):366–75.
- Andrea M, Marquard, Aron C, Eklund, Tejal, Joshi, Marcin, Krzystanek, Francesco, Favero. Pan-cancer analysis of genomic scar signatures associated with homologous recombination deficiency suggests novel indications for existing cancer drugs. *Biomark Res.* 2015;1(3):9.
- Malta TM, Sokolov A, Gentles AJ, Burzykowski T, Poisson L, Weinstein JN. Kamińska B, Huelsken J. Machine Learning Identifies Stemness Features Associated with Oncogenic Dedifferentiation. *Cell.* 2018;173(2):338–54.
- El Bairi K, Afqir S, Amrani M. Is HE4 Superior over CA-125 in the follow-up of patients with epithelial ovarian Cancer? *Curr Drug Targets.* 2020;21(10):1026–33.
- Deng J, Wang L, Chen H, Li L, Ma Y, Ni J, Li Y. The role of tumour-associated MUC1 in epithelial ovarian cancer metastasis and progression. *Cancer Metastasis Reviews.* 2013;32(3–4):535–51.
- Samstein RM, Lee C-H, Shoushtari AN, Hellmann MD, Shen R, Janjigian YY, Baron DA, Zehir A, Jordan EJ, Omuro A, Kaley T J. Tumor mutational load predicts survival after immunotherapy across multiple cancer types. *Nat Genet.* 2019;51(2):202–6.
- Lmsa B, Frhc D, Hwang ED, Botling FJ, Lopez-Rios FF, Lb H, Mk I, Acr J, Mbb D, Ab K. The promises and challenges of Tumor Mutation Burden as an Immunotherapy Biomarker: a perspective from the International Association for the Study of Lung Cancer Pathology Committee. *J Thorac Oncol.* 2020;15(9):1409–24.
- Schrock AB, Ouyang C, Sandhu J, Sokol E, Jin D, Ross JS, Miller VA, Lim D, Amanam I, Chao J. Tumor mutational burden is predictive of response to immune checkpoint inhibitors in MSI-high metastatic colorectal cancer. *Ann Oncol.* 2019;30(7):1096–103.
- Solinas C, Marcoux D, Garaud S, Vitória J, Gert V, Wind AD, Silva PD, Boisson A, Craciun L, Larsimont D. BRCA gene mutations do not shape the extent and organization of tumor infiltrating lymphocytes in triple negative breast cancer. *Cancer Lett.* 2019;450:88–97.
- Shim JH, Hong SK, Cha H, Kim S, Lee SH. HLA-corrected tumor mutation burden and homologous recombination deficiency for the prediction of response to PD-(L)1 blockade in advanced non-small-cell lung cancer patients. *Ann Oncol.* 2020;31(7):902–11.
- Luo Y, Xia Y, Liu D, Li X, Li H, Liu J, Zhou D, Dong Y, Li X, Qian Y, Xu C, Tao K, Li G, Pan W, Zhong Q, Liu X, Xu S, Wang Z, Liu R, Zhang W, Shan W, Fang T, Wang S, Peng Z, Jin P, Jin N, Shi S, Chen Y, Wang M, Jiao X, Luo M, Gong W, Wang Y, Yao Y, Zhao Y, Huang X, Ji X, He Z, Zhao G, Liu R, Wu M, Chen G, Hong L, Consortium C, Ma D, Fang Y, Liang H, Gao Q. Neoadjuvant PARPi or chemotherapy in ovarian cancer informs targeting effector Treg cells for homologous-recombination-deficient tumors. *Cell.* 2024;187(18):4905–25. e24.
- Knudsen ES, Kumarasamy V, Chung S, Ruiz A, Vail P, Tzetzso S, Wu J, Nambiar R, Sivinski J, Chauhan S S. Targeting dual signalling pathways in concert with immune checkpoints for the treatment of pancreatic cancer. *Gut.* 2020;70(1):127–38.

33. Wu Y, Wei J, Xia C, Qin Y, Mao R, Jian S, Fan Y. Comprehensive transcriptome profiling in elderly cancer patients reveals aging-altered immune cells and immune checkpoints. *Int J Cancer*. 2019;144(7):1657–63.
34. Janic B, Brown S, Neff R, Liu F, Wen N. Radiation and Gold Nanoparticle increase the expression of immunogenic cell death markers in MDA MB 231 breast Cancer Model. *Int J Rad Oncol Biol Phys*. 2020;108(2):E26–27.
35. Leon-Cabrera S, Schwertfeger K, L, Terrazas. L I. inflammation as a target in Cancer Therapy. *Mediators Inflamm*. 2019;2019:1971698.
36. Su J, Long W, Ma Q, Xiao K, Liu Q. Identification of a Tumor Microenvironment-related eight-gene signature for Predicting Prognosis in Lower-Grade Gliomas. *Front Genet*. 2019;10:1143.
37. Knutson KL, Maurer MJ, Preston CC, Moysich KB, Goergen K, Hawthorne KM, Cunningham JM, Odunsi K, Hartmann LC, Kalli KR, Oberg AL, Goode E L. Regulatory T cells, inherited variation, and clinical outcome in epithelial ovarian cancer. *Cancer Immunol Immunotherapy*. 2015;64(12):1495–504.
38. Curiel TJ, Coukos G, Zou L, Alvarez X, Cheng P, Mottram P, Evdemon-Hogan M, Conejo-Garcia JR, Zhang L, Burow M. Specific recruitment of regulatory T cells in ovarian carcinoma fosters immune privilege and predicts reduced survival. *Nat Med*. 2004;10(9):942–9.
39. Gaowen C, Lin Z, Yulu Y, Yusheng L, Xiangyuan L, Yifeng W. Prognostic role of neutrophil to lymphocyte ratio in ovarian Cancer: a Meta-analysis. *Technol Cancer Res Treat*. 2018;17:153303381879150.
40. Yang L, Liu Q, Zhang X, Liu X, Song E. DNA of neutrophil extracellular traps promotes cancer metastasis via CCDC25. *Nature*. 2020;583(7814):133–8.
41. Ogawa R, Yamamoto T, Hirai H, Hanada K, Kiyasu Y, Nishikawa G, Mizuno R, Inamoto S, Itatani Y, Sakai Y. Loss of SMAD4 promotes colorectal cancer progression by recruiting tumor-associated neutrophils via CXCL1/8-CXCR2 axis. *Clin Cancer Res*. 2019;25(9):2887–99.
42. Peter. LangfelderSteve, Horvath. WGCNA: an R package for weighted correlation network analysis. *BMC Bioinformatics*. 2008;9:559.
43. Elkins K, Zheng B, Go M, Slaga D, Du C, Scales SJ, Yu SF, McBride J, De Tute. R, Rawstron A. FcRL5 as a target of antibody–drug conjugates for the treatment of multiple myeloma. *Mol Cancer Ther*. 2012;11(10):2222–32.
44. Liu Y, Chen Y, Hu X, Meng J, Li X. Development and validation of the B Cell-Associated fc receptor-like molecule-based prognostic signature in skin cutaneous melanoma. *Biomed Res Int*. 2020;2020(1):1–11.

### Publisher's note

Springer Nature remains neutral with regard to jurisdictional claims in published maps and institutional affiliations.